MIMO SLIDING-MODE AND H∞ CONTROLLER DESIGN FOR DYNAMIC COUPLING REDUCTION IN UNDERWATER-MANIPULATOR SYSTEMS

Serdar Soylu*, Bradley J. Buckham, and Ron P. Podhorodeski
Department of Mechanical Engineering,
University of Victoria, P.O. Box 3055, Victoria, B.C., Canada, V8W 3P6
{serdar, bbuckham, podhoro}@me.uvic.ca
*Corresponding author: Fax: (250) 721-6035

Abstract

In underwater remote vehicle-manipulator system (**URVM**) applications, it is beneficial to have the underwater remote vehicle (**URV**) hold station using its thrusters while a human pilot operates the serial manipulator. This provides a stable platform for the manipulator and eases the pilot's job drastically when current and/or tether disturbances are present. In this work, the reduction of dynamic coupling in the URVM systems is realized using two robust control techniques namely Sliding-mode control and H_∞ control, and the performance of both controllers in the dynamic coupling reduction problem is reported. In addition, a new control scheme is proposed that involves both controllers in the control loop. Numerical case studies are developed to demonstrate the effectiveness of the controllers. It is concluded that sliding-mode and H_∞ controller combined approach provides superior dynamic coupling reduction performance.

Résumé

Pour des applications de systèmes de manipulateur-véhicule sous-marin télécommandés (MVST), il est bénéfique que le véhicule sous-marin télécommandé (VST) maintienne sa position avec ses propulseurs tandis qu'un pilote humain actionne le manipulateur sériel. Cela fournit une plate-forme stable pour le manipulateur et facilite grandement la tâche du pilote en présence de perturbations dues au courant et/ou au cordon ombilical. Dans ce travail, une réduction du couplage dynamique dans les systèmes MVST est réalisée en utilisant deux méthodes de commande robustes, soit la commande par mode de glissement et la commande H_∞. La performance des deux systèmes de commande pour la réduction du couplage dynamique est présentée. De plus, une nouvelle approche qui comprend les deux systèmes dans la boucle de commande est proposée. Des études de cas numériques sont développées afin de démontrer l'efficacité des systèmes de commande. Il est conclu que l'approche combinant la commande par mode de glissement et la commande H_∞ offre une performance supérieure pour diminuer le couplage dynamique.

1   INTRODUCTION

In many URV applications, a master-slave configuration is used to operate the manipulator. In this configuration, the movement of the smaller master arm driven by an operator on a surface support vessel, is approximately duplicated by the larger slave arm relative to the URV frame of reference [1]. However, when the movement is replicated by the larger-slave arm, a force is exerted on the vehicle through dynamic coupling. Since the end effector's position and orientation are a function of accumulated URV motions, this disturbance of the URV state adversely affects the end-effector position and orientation; the slave arm end-effector does not achieve the same final state as the master arm [1].   Nonlinear hydrodynamic effects dominant the coupled vehicle-manipulator dynamics and the hydrodynamics vary greatly with changes in arm and vehicle orientation [2]. Consequently, reducing the negative effect of the dynamic coupling present in the URV manipulator system through the use of on-board controllers becomes a significant issue in obtaining better system performance [3].

Several control methods have been applied to control URV motion. Yoerger and Slotine [4] applied Slotine's [5] sliding-mode methodology to the control problem of the URV. In [4], a series of single-input single-output controllers were used, and the robustness of the control scheme was demonstrated. Cristi *et al.* [6] proposed a control technique that combines the robustness property of the sliding-mode controller with the adaptivity of an adaptive controller. Yuh [7] demonstrated the application of neural networks to an underwater robotic control system, and concluded that a neural network controller provides a robust control technique in case the exact dynamic knowledge is not available. Dunnigan and Russel [8] addressed the dynamic coupling problem for URVM systems, and proposed the sliding-mode approach in an effort to keep a URV stationary. The sliding-mode control methodology was also utilized to solve the URVM dynamic coupling problem in [8] in which an accurate dynamic coupling prediction required inertial measurement units for monitoring the URV motion. In [9], the Articulated-Body Algorithm (**ABA**) predicted the dynamic coupling force expressions based on the feedback of the URV and the manipulator states. It was shown in the same paper that using the ABA not only eliminates the need for an inertial sensor, but it also produces better dynamic coupling reduction performance.

The H_∞ approach is applied in [10] to the problem of precise trajectory controlling. To this end, the nonlinear system dynamics were linearized around an operating point, and standard techniques of H_∞ theory [11] were applied. Conte and Serrani [12] proposed a scheduling of linear H_∞ controllers, and simulation studies were carried out for a broad range of operating conditions. They showed that the H_∞ approach provides a robust control technique for the control of underwater vehicles. In [13], Conte *et al.* considered the problem of decoupling the effect of the umbilical's traction from the position of a URV. It is shown in [13] that the full disturbance decoupling is theoretically not possible within the H_∞ controller synthesis theory. However, the almost disturbance decoupling was proved to be theoretically realizable in the same work. An H_∞ autopilot design for an autonomous underwater vehicle is presented in [14]. The design of sub-controllers is formulated as the problem of minimizing the mixed sensitivity function, and is solved by the Linear Matrix Inequality (**LMI**)-based H_∞ method. In [15], the same problem was solved using reduced-order H_∞ synthesis that produces reduced-order controllers with slight performance degradation compared to LMI-based controllers.

The primary goal of the current proposed research is to compare the ability of sliding-mode H_∞ controllers to attenuate the dynamic coupling in URVM systems, and to propose a control scheme that combines the two controller methodology to further improve the controller performance.

2   MODELLING

2.1   Vehicle Modelling with Newton-Euler Dynamics

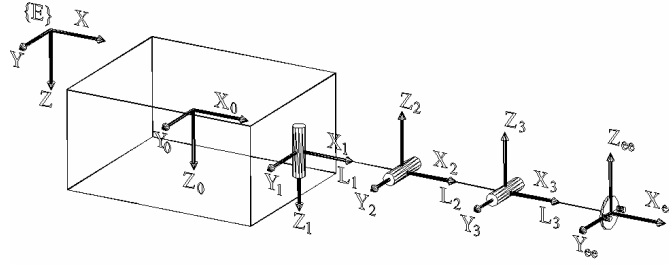The general kinematics characteristics of the URVM system are presented below.

Figure 1: URVM system.

As shown in Figure 1, the Z axis of the earth-fixed inertial frame *{E}* is assumed in the gravity direction as is consistent with traditional marine mechanics. The URV is modeled as another manipulator link in the serial chain and numbered as *0*. The body-fixed frame is attached to the centre of mass of the URV as shown in Figure 1. The URV spatial velocity state vector with respect to (**wrt**) its body-fixed frame is considered to be $\boldsymbol{\mu} = [\mathbf{v}_1 \quad \mathbf{v}_2]^T = [p \quad q \quad r \quad u \quad v \quad w]^T$ and the position and orientation state vector of the URV wrt the inertial frame is given by $\mathbf{x} = [\phi \quad \theta \quad \psi \quad X \quad Y \quad Z]^T$. The spatial transformation matrix between the inertial frame and URV's body-fixed frame is given by $\mathbf{T} \in \mathbb{R}^{6 \times 6}$, which includes the angular velocity transformation matrix and the linear velocity transformation matrix. The term $\mathbf{T}$ can be obtained by the Euler sequence of rotations [16].

The nonlinear equations of motion of the URV in terms of its body-fixed frame are obtained by applying a Newton-Euler dynamics formulation:

$$\mathbf{M}\dot{\boldsymbol{\mu}} + \mathbf{C}(\boldsymbol{\mu})\boldsymbol{\mu} + \mathbf{D}(\boldsymbol{\mu})\boldsymbol{\mu} + \mathbf{G} = \boldsymbol{\tau}, \quad \dot{\mathbf{x}} = \mathbf{T}\boldsymbol{\mu} \qquad (1)$$

where $\mathbf{M} \in \mathbb{R}^{6 \times 6}$ is the inertia matrix including the added mass effect, $\mathbf{C} \in \mathbb{R}^{6 \times 6}$ is the Coriolis matrix that results from the use of a local frame attached to the URV, $\mathbf{D} \in \mathbb{R}^{6 \times 6}$ is the damping matrix, $\mathbf{G} \in \mathbb{R}^6$ is the gravity matrix, and finally $\boldsymbol{\tau} \in \mathbb{R}^6$ is the force and moment vector acting on the system including thrusters forces, tether forces and the manipulator disturbance forces. The definitions of these terms can be found in [16].

2.2 Linearized Model

To be able to implement H_∞ control theory, the nonlinear system must be linearized around a specific operating point. To this end, the linear model can be obtained by linearization of the general expression given in Eq. (1). Since our main goal is to keep the URV stationary in the presence of the disturbances, the operating point or equilibrium point must be **0**. The linearization process around the operating point of **0** yields the following linear time-invariant (**LTI**) system [16]:

$$\begin{bmatrix} \Delta\dot{\boldsymbol{\mu}} \\ \Delta\dot{\mathbf{x}} \end{bmatrix} = \begin{bmatrix} -\mathbf{M}^{-1}\mathbf{D} & -\mathbf{M}^{-1} \\ \mathbf{T} & \mathbf{0}_{6\times6} \end{bmatrix} \begin{bmatrix} \Delta\boldsymbol{\mu} \\ \Delta\mathbf{x} \end{bmatrix} + \begin{bmatrix} \mathbf{M}^{-1} \\ \mathbf{0}_{6\times6} \end{bmatrix} \begin{bmatrix} \mathbf{u} \\ \mathbf{0}_{6\times1} \end{bmatrix} \qquad (2)$$

Eq. (2) can be written in a compact form as follows:

$$\dot{\boldsymbol{\xi}} = \mathbf{A}\boldsymbol{\xi} + \mathbf{B}\mathbf{u} \qquad (3)$$

To complete the linear model, the output of the system can be given as:

$$\Delta\mathbf{y} = \mathbf{C}\boldsymbol{\xi} \qquad (4)$$

3   CONTROL

3.1   MIMO Sliding Mode Control

A multi-input multi-output model-based sliding mode controller allows using one centralized controller instead of many, i.e., one for each controlled axis. The centralized controller coordinates the URV motion in such a way that the desired task is accomplished.

The design of a sliding mode control follows two main steps. First one designs a switching surface $\mathbf{s}$ to represent a desired system dynamics, then a control law $\mathbf{u} \in \mathbb{R}^6$ is designed that drives the system states on to the switching surface $\mathbf{s} \in \mathbb{R}^6$ in a finite time and keeps them on the surface until they hit the desired location on the surface in spite of parameter changes and disturbances [5].

The vector of sliding surfaces $\mathbf{s}$ is defined as:

$$\mathbf{s} = \Upsilon \begin{bmatrix} {}^B_I \mathbf{R} \tilde{\boldsymbol{\eta}} \\ \tilde{\boldsymbol{\eta}}_2 \end{bmatrix} - \begin{bmatrix} \mathbf{v}_1 \\ \mathbf{v}_2 \end{bmatrix} = \mathbf{r} - \boldsymbol{\mu} \tag{5}$$

where $\Upsilon \in \mathbb{R}^{6 \times 6}$ is a positive definite matrix containing the control bandwidth value for each sliding surface, ${}^B_I \mathbf{R} \in \mathbb{R}^{3 \times 3}$ is the rotation matrix from the inertial frame to the body-fixed frame, and the rest of the terms in Eq. (5) are defined as with subscript d denoting the desired values:

$$\tilde{\boldsymbol{\eta}}_1 = \begin{bmatrix} x_d - x & y_d - y & z_d - z \end{bmatrix}^T, \tilde{\boldsymbol{\eta}}_2 = \begin{bmatrix} \phi_d - \phi & \theta_d - \theta & \psi_d - \psi \end{bmatrix}^T \tag{6}$$

The following control law is implemented based on the work of [17].

$$\mathbf{u} = \mathbf{B}^\dagger \left[\mathbf{K}_D \mathbf{s} + \hat{\mathbf{M}} \dot{\mathbf{r}} + \left(\hat{\mathbf{C}} + \hat{\mathbf{D}} \right) \mathbf{r} + \hat{\mathbf{G}} + \mathbf{K}_s sat(\mathbf{s}/\Phi) \right] \tag{7}$$

where $\mathbf{B}^\dagger$ is the pseudoinverse of matrix $\mathbf{B}$, $\mathbf{K}_D \in \mathbb{R}^{6 \times 6}$ is a positive definite matrix of gains, $\hat{\mathbf{M}}$, $\hat{\mathbf{C}}$, $\hat{\mathbf{D}}$ and $\hat{\mathbf{G}}$ are the estimates of inertia matrix $\mathbf{M}$, the vector of Coriolis and centripetal acceleration $\mathbf{C}$, the vector of dissipative effects, and gravitational and buoyant force $\mathbf{G}$, respectively. The term $\mathbf{K}_s \in \mathbb{R}^{6 \times 6}$ is a positive definite matrix, and $sat(\mathbf{s})$ is the saturation function [16].

Theorem 1: *Consider the nonlinear dynamical system described by Eq. (1). If the control law is expressed as Eq. (7) then stability of the closed-loop control system is guaranteed in Lyapunov sense with $1/2 \mathbf{s}^T \mathbf{M} \mathbf{s}$ being a Lyapunov function candidate.*

Proof: See Antonelli [17].

3.2   H∞ Control Design

A typical feedback system is demonstrated in Figure 2 in which $\mathbf{K}$ is the controller, $\mathbf{G}$ is the system that is to be controlled, and $\mathbf{d}$ is a disturbance. The term $\mathbf{r}$ represents the reference input that is supposed to be tracked by the system, $\mathbf{e}$ is the error between the reference input and the system output, and finally $\mathbf{u}$ is the control input produced by the controller $\mathbf{K}$.
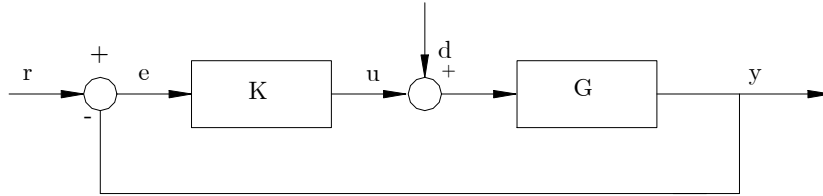

Figure 2: Feedback control loop. The input disturbance force is given by d.

H∞ design software programs usually require the system to be expressed in a so-called interconnection system, which is the state-space representation of the augmented system. Such a structure can be easily

obtained by adding the performance weighting functions $\mathbf{W_P}$ that captures the closed-loop performance specifications (minimum bandwidth frequency, maximum steady state error, and maximum peak magnitude) and robust weighting function $\mathbf{W_r}$ that characterizes the known frequency dependent knowledge of the modelling uncertainty [11]-[18]. The resulting the feedback control loop and the augmented plant $\mathbf{P}$ are demonstrated in Figure 3.
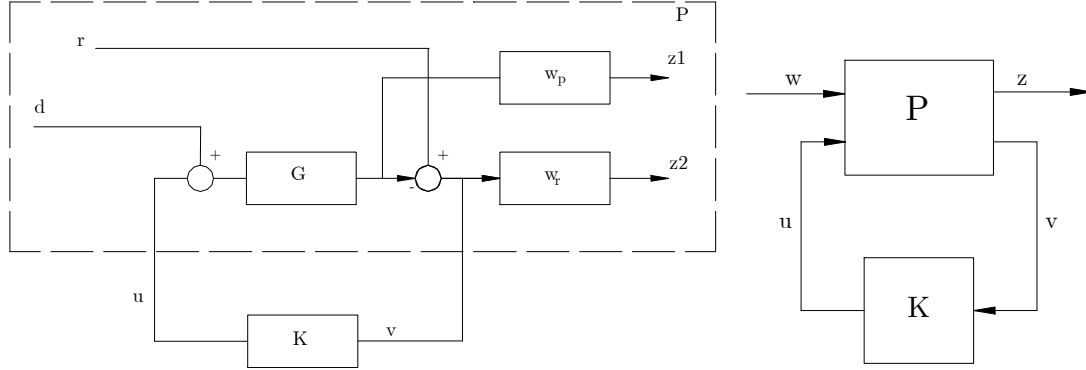

Figure 3: Feedback control loop (left) and Augmented plant P (right).

So the augmented plant $\mathbf{P}$ from $[\mathbf{w},\mathbf{u}]^T$ to $[\mathbf{z},\mathbf{v}]^T$ is

$$\begin{bmatrix} \mathbf{z} \\ \mathbf{v} \end{bmatrix} = \begin{bmatrix} \mathbf{P}_{11}(j\omega) & \mathbf{P}_{12}(j\omega) \\ \mathbf{P}_{21}(j\omega) & \mathbf{P}_{22}(j\omega) \end{bmatrix} \begin{bmatrix} \mathbf{w} \\ \mathbf{u} \end{bmatrix}, \ \mathbf{u} = \mathbf{K}(j\omega)\mathbf{v} \tag{8}$$

where $\mathbf{z} = [\mathbf{z}_1 \quad \mathbf{z}_2]^T$ with $\mathbf{z}_1 = w_p \mathbf{u}$ and $\mathbf{z}_2 = w_r \mathbf{Gu}$, $\mathbf{w} = [\mathbf{r} \quad \mathbf{d}]$, $\mathbf{v} = \mathbf{w} - \mathbf{Gu}$ and

$$\mathbf{P}_{11}(j\omega) = \begin{bmatrix} w_r \mathbf{I} & -w_p(j\omega)\mathbf{G}(j\omega) \\ \mathbf{0} & w_r(j\omega)\mathbf{G}(j\omega) \end{bmatrix} \begin{bmatrix} w_p(j\omega)\mathbf{I} \\ \mathbf{0} \end{bmatrix}, \mathbf{P}_{12}(j\omega) = \begin{bmatrix} -w_p(j\omega)\mathbf{G}(j\omega) \\ w_r(j\omega)\mathbf{G}(j\omega) \end{bmatrix} \tag{9}$$

$$\mathbf{P}_{21}(j\omega) = \begin{bmatrix} \mathbf{I} & -\mathbf{G}(j\omega) \end{bmatrix}\mathbf{I}, \mathbf{P}_{22}(j\omega) = -\mathbf{G}(j\omega)$$

The major goal of the H$_\infty$ design method is to minimize the effect of the worst-case disturbance $\mathbf{w}$ on the output $\mathbf{z}$. The cost function to be minimized is defined as the transfer function between $\mathbf{w}$ and $\mathbf{z}$, and is expressed as $\mathbf{T}_{zw} = \mathbf{P}_{11} + \mathbf{P}_{12}(\mathbf{I} - \mathbf{P}_{22}\mathbf{K})^{-1}\mathbf{K}\mathbf{P}_{21}$ yielding:

$$\mathbf{T}_{zw} = \begin{bmatrix} \mathbf{0} & -w_p(j\omega)\mathbf{G}(j\omega) \\ w_r(j\omega) & w_r(j\omega)\mathbf{G}(j\omega) \end{bmatrix} + \begin{bmatrix} -w_p(j\omega)\mathbf{G}(j\omega) \\ w_r(j\omega)\mathbf{G}(j\omega) \end{bmatrix}\mathbf{K}(\mathbf{I} + \mathbf{GK})^{-1}\begin{bmatrix} \mathbf{I} & -\mathbf{G}(j\omega) \end{bmatrix} = \begin{bmatrix} (\mathbf{S}(j\omega)w_p(j\omega)) \\ (\mathbf{T}(j\omega)w_r(j\omega)) \end{bmatrix} \tag{10}$$

In Eq. (10) γ is a constant called nominal performance bound that represens the desired performance level of the closed-loop system and the terms $\mathbf{S}$ and $\mathbf{T}$ are called the sensitivity function, and complimentary sensitivity function, respectively [18]. The H$_\infty$ design process seeks a controller $\mathbf{K}$ such that the closed-loop gain $\mathbf{T}_{zw}$ is minimized in the sense of the H$_\infty$ norm while maintaining internal stability. That is, ensure $\|\mathbf{T}_{zw}\|_\infty < \gamma$ where the term γ represents the achievable performance level of the closed-loop system for a given set of controller design constraints, and is the result of the optimization problem of $\min\|\mathbf{T}_{zw}\|_\infty$ [11].

Consequently, the problem definition can be given as $\|\mathbf{T}_{zw}\|_\infty = \sup_\omega \bar{\sigma}(\mathbf{T}_{zw}(j\omega))$ where $\|\mathbf{T}_{zw}\|_\infty$ is called the mixed-sensitivity cost function, $\bar{\sigma}(.)$ is the maximum singular value and $\sup_\omega$ implies supremum, or least upper bound [11].

In the H_∞ framework, the desired controller performance is given as frequency domain specifications on the various closed-loop transfer functions. These frequency domain specifications form design constraints on the gain response of the closed-loop transfer functions within the H_∞ control problem. The procedure of defining the frequency domain specifications such as tracking performance, disturbance rejection, roll-off, robustness to model uncertainty is called loop shaping [11]. The performance specification and the robustness specification require the following inequalities to hold:

$$\bar{\sigma}(\mathbf{S}(j\omega)w_p(j\omega)) \leq 1, \quad \bar{\sigma}(\mathbf{T}(j\omega)w_r(j\omega)) \leq 1 \tag{11}$$

These performance and robustness specifications can be lumped into the following infinity norm inequality:

$$\|\mathbf{T}_{zw}\|_\infty = \left\| \begin{pmatrix} \mathbf{S}(j\omega)w_p(j\omega) \\ \mathbf{T}(j\omega)w_r(j\omega) \end{pmatrix} \right\|_\infty \leq 1 \tag{12}$$

as a result of the following inequalities:

$$\max\left\{ \bar{\sigma}(\mathbf{S}(j\omega)w_p(j\omega)), \bar{\sigma}(\mathbf{T}(j\omega)w_r(j\omega)) \right\} \leq \bar{\sigma}\left(\begin{bmatrix} \mathbf{S}(j\omega)w_p(j\omega) \\ \mathbf{T}(j\omega)w_r(j\omega) \end{bmatrix} \right) \leq \left\| \begin{matrix} \mathbf{S}(j\omega)w_p(j\omega) \\ \mathbf{T}(j\omega)w_r(j\omega) \end{matrix} \right\|_\infty \tag{13}$$

3.3 Weighting Function Selection

In the current work, the performance weighting function for the control system was chosen based on the work of [14] as:

$$w_p = 10(l+10)/1000l+1 \tag{14}$$

with l indicating the Laplace domain. This choice leads the steady state error to be below 1%.

The robustness weighting function w_r represents the bound on this uncertainty term. It is assumed that the neglected high frequency dynamics cause as much as 40 dB deviation between the frequency response of the linearized model and the actual system for frequencies over 0.5 Hz. This requires 40dB/dec attenuation after 0.5Hz. The robustness bound satisfying the said conditions was chosen to be:

$$w_r = l^2/10 \tag{15}$$

Note that although w_r is improper, the augmented plant is proper since $w_r(j\omega)\mathbf{G}(j\omega)$ is proper, and that it does not lead to an ill-conditioned state matrix in the realization of the augmented plant $\mathbf{P}$ [11].

3.4 Solution Procedure

For synthesis of the H_∞ control, transfer matrix $\mathbf{G}$ in Eq.(8) is replaced by $\mathbf{C}_l(s\mathbf{I}\text{-}\mathbf{A}_l)^{-1}\mathbf{B}_l$, which is the transfer matrix of the linear model given in Eqs. (3)-(4). The weighting functions are defined based on the design specifications. There are two common approaches to solve the problem of the minimization of the cost fuction, i.e., $\min\|\mathbf{T}_{zw}\|_\infty$; the Riccati-Based and the LMI-based. The LMI-based H_∞ control theory [19] will be utilized to synthesize the controller since it applies directly to singular plants. This is the case for our system since the eigenvalue analysis reveals that the linearized model of the vehicle has poles at the origin.

4   SIMULATION RESULTS

4.1   System Overview

These two controllers were applied to the full nonlinear plant, and their performances in the attenuation of the dynamic coupling were evaluated. The URVM system considered in this work is Canadian Scientific Submersible Facility (ROPOS) [20], and all the associated parameters used in this simulation study are given in [20]. The current ROPOS system does not involve manipulators, and hence manipulators from [21] were used instead; these manipulators were chosen due to the similarities in dimensions of their vehicles and the vehicles used in the ROPOS system. In the simulation, a station keeping task is considered for the URV whose initial orientation and position vector is zero. Likewise, the initial configuration of the manipulator is also taken as zero. A randomly selected torque vector of $\tau = \begin{bmatrix} 40 & 0 & 0 \end{bmatrix}$ Nm, which corresponds to the pilot's true desire during task execution and could be any value, is applied for 60 seconds. No joint displacement limit is considered in the current simulation study. The applied torque vector creates constant disturbance to the URV motion through reaction forces and moments at the junction point between the URV and the manipulator, and in turn causes changes in the position and orientation of the URV. These effects leads to the reduction of task effectiveness, and must be compensated for in order to obtain better system performance in underwater robotic applications. The compensation of the reaction forces and moments will be given by controllers.   In underwater applications, these compensation forces and moments are applied to the system by means of thrusters. For the thruster dynamics, a simplified first-order model of the thrusters was implemented. The first-order dynamics successfully model the lag between the controller's commanded thrust and the actual thrust through a time-constant term. The dimensionless time constant term is considered to be 0.07. This value successfully reflects the time lag behaviour of conventional thrusters and is determined based on trial and error. In addition, it will be assumed that commanded thrusts are applied directly to the center of mass of the URV. In order to model uncertainties in the dynamics parameters, drag and added mass coefficients of the URV differed from the real system by 20%. Success of the controller in the presence of these parameter perturbations will partly address the issue of controller robustness. *MatLab Simulink* software was used to perform the simulation. As an integrator, *ode15s* is used.

To predict the reaction forces and moments at the junction point, the ABA [22] algorithm is used in the simulation studies.

4.2   Sliding-Mode Control

MIMO sliding-mode controller has been synthesized based on Section 3.1.   The control law parameters were chosen by trial and error to be: $\Upsilon = \begin{bmatrix} 0.5 & 0.5 & 0.5 & 0.5 & 0.5 & 0.5 \end{bmatrix}^T$ and $\mathbf{K}_D = \begin{bmatrix} 10 & 10 & 10 & 10 & 10 & 10 \end{bmatrix}^T$. Differently from the general approach in which control parameter $\mathbf{K}_S$ is taken as constant, in the current implementation of the MIMO sliding-mode controller, the term $\mathbf{K}_S$ is updated using **SVD** (Singular Value Decomposition) so that the convergence condition given in [17] is guaranteed to be satisfied by the sliding-mode controller during task execution.   Boundary layer parameter Φ has been set to 0.2 to prevent the chattering problem.

Dynamic simulations were performed for 60 seconds, and the reaction forces and moments occuring at the junction point between the vehicle and the manipulator are demonstrated in Figure 4. The MIMO sliding-mode controller tries to compensate these disturbance forces and moments by commanding the thrusters. Figure 5 demonstrates the commanded forces and moments at the center of mass of the URV.

Figure 6 reveals the controller performance in keeping the vehicle still. From Figure 6, it can be concluded that the MIMO sliding-mode control technique provides satisfactory station-keeping

performance since the position and orientation error of the URV under the disturbance of the manipulator motion is small.
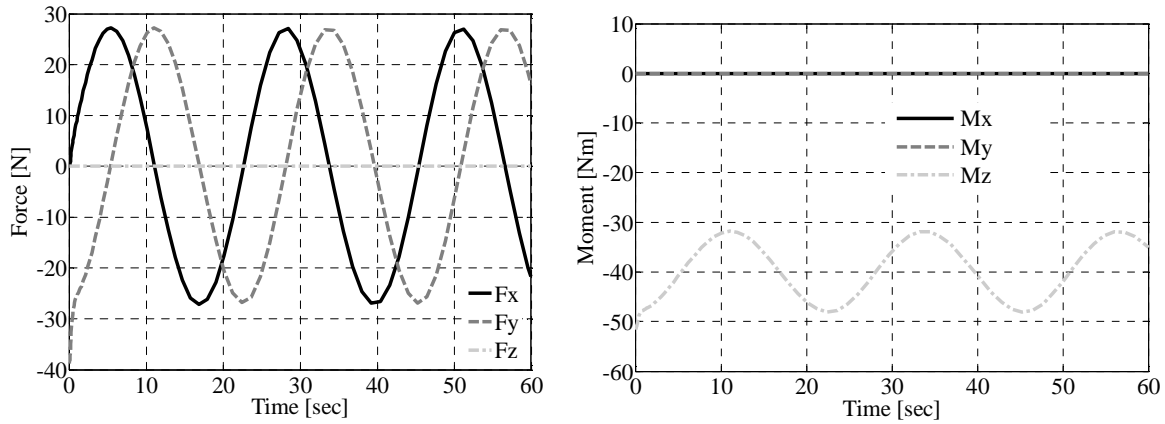

Figure 4: Forces and moments occur at the connection point due to the manipulator motion.
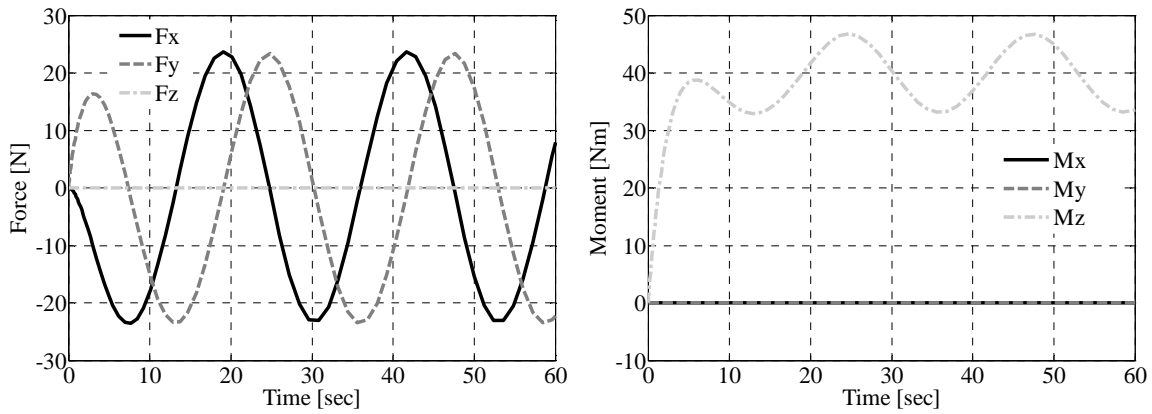

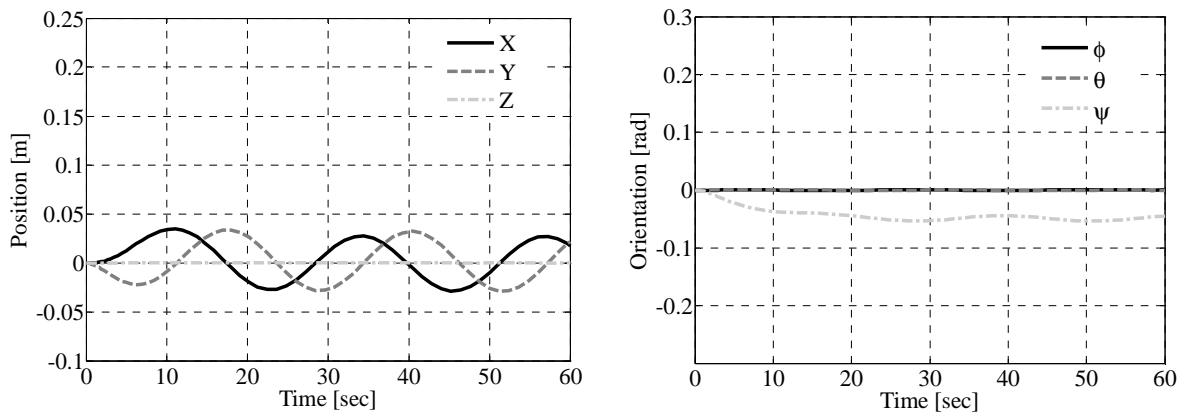Figure 5: The compensation forces and moments

Figure 6: Above two plots demonstrate the URV's translational motion along X, Y and Z axis with respect to the earth reference frame with the sliding mode controller off and on, respectively. These two graphs are also equivalent to the position error of the URV, as zero is the reference value for each degree of freedom of the URV.

4.3   H∞ Controller Synthesis

The H$_\infty$ control technique was applied to the dynamic coupling reduction problem under the simulation parameters as the previous section. To this end, the dynamic coupling term is included into the general problem setting of H$_\infty$ design as outlined in Section 3.4. MatLab's *LMI Control Toolbox* [23] was used to solve the derived LMI equation, Eq (10), through the augmented plant given in Eq. (8). The performance specifications were enforced through the weighting functions defined in Section.3.3. The *LMI Control Toolbox* found an optimal 6-input/6-output controller of 17th order for given design specifications with nominal performance bound $\gamma = 0.2955$.

Figure 7 shows the translational and rotational position error for the H$_\infty$ controller. Figure 7 reveals that H$_\infty$ control synthesis yields a controller that provides satisfactory station-keeping performance. From the figure, it can be concluded that the sliding-mode controller gives slightly better performance in the attenuation of the dynamic coupling effect compared to the H$_\infty$ controller.
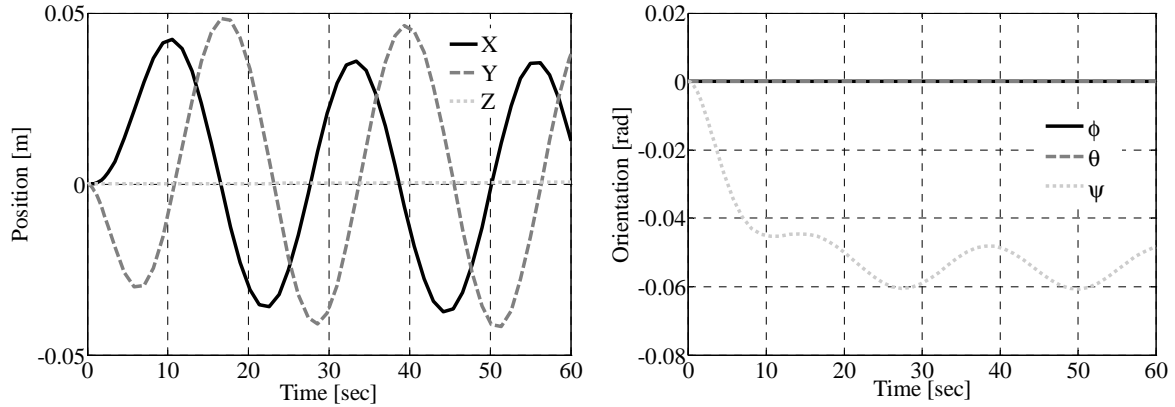

Figure 7: Position and orientation error of the URV due to the manipulator disturbance forces and moments.

4.4   Sliding-Mode - H∞ Controller

In order to further improve the disturbance rejection capability, the two approaches can be combined. The proposed feedback control scheme is given in Figure 8.
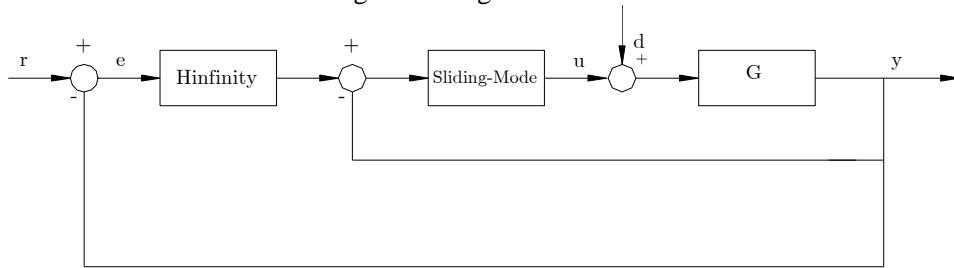

Figure 8: Proposed H$_\infty$ -Sliding-Mode control scheme.

In this proposed scheme, there are two loops. The inner loop consists of the sliding mode controller, the disturbances and the URV dynamics and the outer loop consists of an H$_\infty$ controller. In the inner loop, the low-level sliding mode controller works to drive the state of the nonlinear URV system towards the equilibrium state of **0**. Therefore, the high-level H$_\infty$ controller works on a system whose dynamics model is more consistent with the linearized model used to synthesize the H$_\infty$ controller.

Figure 9 demonstrates the position and orientation error of the URV under the manipulator disturbance. As can be seen from the figure, the combined H$_\infty$-Sliding-Mode controller gives very satisfactory results in keeping the URV's location at zero.

In order to evaluate each controller performance with respect to each other, one should evaluate the Euclidean norm of position and orientation error for each controller. Figure 10 reveals that the combined H_∞-Sliding-Mode controller outperforms the other two controllers. When the area underneath each curve in Figure 10 is considered, the combined H_∞-Sliding-Mode controller improves the position and orientation error as much as 35% and 47%, respectively, compared to the sliding-mode controller alone, and 49% and 49% compared to the H_∞ controller alone.
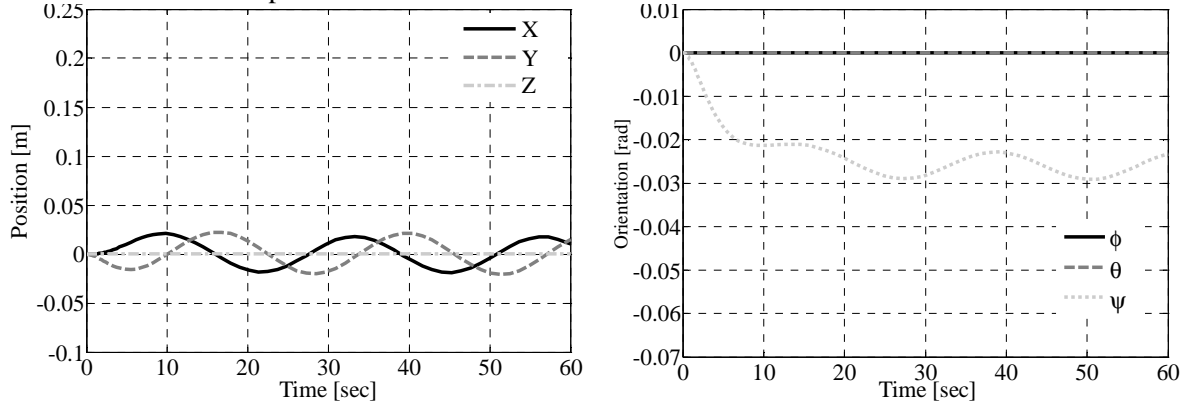

Figure 9: Position and orientation error of the URV due to the manipulator disturbance forces and moments for the combined H_∞-sliding-mode controller.
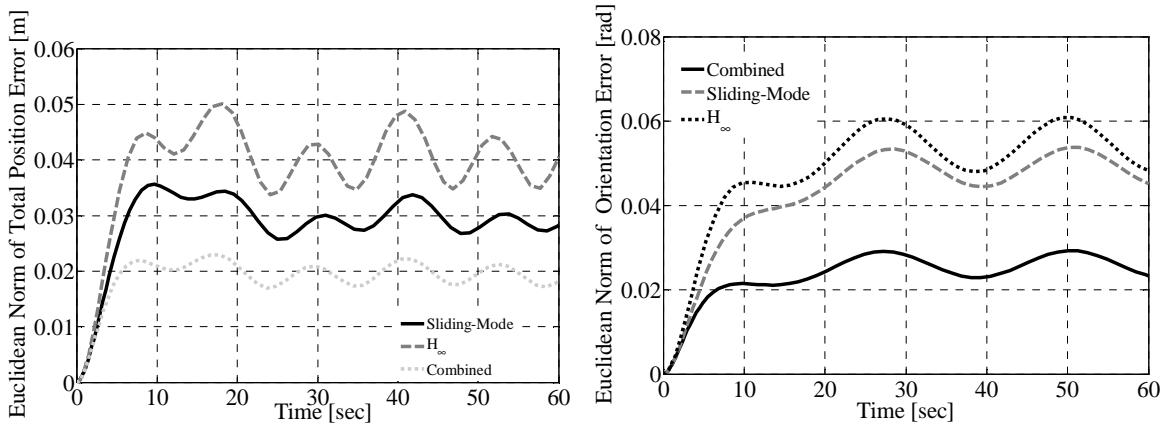

Figure 10: Euclidean norm of position and orientation error for each controller. As can be seen form the figure that the combined H_∞-Sliding-Mode controller outperforms the other two controllers.

5   CONCLUSION

The contribution of this work is twofold. Firstly, the implementation of H_∞ technique to the problem of dynamic coupling reduction in URVMs, and its application to the disturbance mitigation problem is considered to be a unique contribution. Secondly, a new control scheme consisting of a combined sliding-mode and H_∞ controller has been presented. A comparison case study has been developed to evaluate the performance of each controller in the dynamic coupling reduction problem. Results have demonstrated that the combined H_∞-Sliding-Mode controller outperforms the other two controllers. This improvement can be attributed to the fact that, the high-level H_∞ controller works on a system whose dynamics model is more consistent with the linearized model used to synthesize the $H\infty$ controller due to the low level sliding-mode controller. Although the performance evaluation of each controller has been

performed exclusively for the dynamic coupling reduction problem, the proposed control scheme can be easily extended to other URV problems such as waypoint navigation.

ACKNOWLEDGEMENT

REFERENCES

[1] D. M. Lane, M. W. Dunnigan, P. J. Knightbridge, and A.W. Quinn, "Planning and control for co-ordination of underwater manipulators," *Proc. IEE Control 91*, pp. 493-498, 1991.

[2] J. H. Ryu, D. S. Kwon, and P. M. Lee, "Control of underwater manipulators mounted on an ROV using base force information," *IEEE International Conference on Robotics & Automation*, pp. 3238-3243, May 2001.

[3] J. Yuh, "Modeling and control of underwater robotic Vehicles," *IEEE Trans. Syst., Man, Cybern.*, vol. 20, pp. 1475-1483, 1990.

[4] D. Yoerger, and J. J. E. Slotine, "Robust trajectory control of underwater vehicles," *IEEE J. Ocean Eng.,* vol. OE-10, pp. 462-470, Oct. 1985.

[5] J. J. E. Slotine, and L. Weiping, *Applied Nonlinear Control*, Prentice-Hall, 1991.

[6] R. Cristi, F. A. Papoulias, A. J. Healey, "Adaptive sliding mode control of autonomous underwater vehicles in the dive plane," *IEEE J. Oceanic Eng.*, vol. 15, no. 3, pp. 152-160, July 1990.

[7] J. Yuh, "A neural net controller for underwater robotic vehicles," *IEEE J. Oceanic Eng.*, vol. 15, no. 3, pp. 327-339, 1993.

[8] M. W. Dunnigan, and G. T. Russell, "Evaluation and reduction of the dynamic coupling between a manipulator and an underwater vehicle," *IEEE Journal of Oceanic Engineering*, vol. 23, no. 3, pp. 260-273, July 1998.

[9] S. Soylu, B. J. Buckham and R. P. Podhorodeski, "Using articulated-body algorithm within sliding mode control to compensate dynamic coupling in underwater manipulator systems," *CSME Trans.* vol. 29, no. 4, pp. 629-643, 2005.

[10] I. Kaminer and A. M. Pascoal, "Control of an underwater vehicle using H_∞ synthesis", *Proc. 30th IEEE CDC*, pp.2350-2355,1991.

[11] K. Zhuo, Essentials of robust control, Prentice-Hall, 1998.

[12] G. Conte and A. Serrani, "Robust control of a remotely operated underwater vehicle," *Automatica,* vol.34, no. 2, pp. 193-198, 1998.

[13] G. Conte, A. Serrani, and A.M. Perdon, "Rejecting the disturbances due to the umbilical's traction in ROVs' control," *In Proceedings of IEEE Oceans '98*, Nice, France, 1998.

[14] Z. Feng and R. Allen, "H_∞ autopilot design for an autonomous underwater vehicle, " *In Proceedings of IEEE International Conference on Control Applications,* Glaskow, Scotland, UK, 2002.

[15] Z. Feng and R. Allen, "Reduced order H_∞ control of an autonomous underwater vehicle," *Control Engineering Practice*, vol.13, pp. 1511-1520, 2004.

[16] T. Fossen, Guidance and Control of Ocean Vehicles, Wiley, 1994.

[17] G. Antonelli G., Underwater Robots: Motion and force control of vehicle-manipulator systems. Springer-Verlag, 2003.

[18] J. C. Doyle and G. Stein, Multivariable feedback design-concept for a classical/modern synthesis, *IEEE Trans. Automat. Control.* vol AC 26, no.1, pp.4-16.

[19] P. Gahinet and P. Apkarian, "A linear matrix inequality approach to H_∞ control," *International Journal of Robust Nonlinear Control,* vol. 4, pp.421-448, 1994.

[20] B. Buckham, D. Steinke, and S. Prabhakar, ''Evaluation of the ROPOS Liveboating Configuration Using Dynamic Simulation," *in Proceedings of CANCAM 2005 (20th Canadian Congress of Applied Mechanics),* Montreal, QC, Canada.

[21] T. K. Podder, "Dynamics and control of kinematically redundant underwater vehicle-manipulatror systems. Autonomus System Laboratory Technical Report, ASL 98-01, University of Hawaii, Honolulu, Hawaii Adaptive control of an autonomous underwater vehicle,1998.

[22] S. McMillan, D. E. Orin, and R. B. McGhee, "Efficient dynamic simulation of an underwater vehicle with a robotic manipulator," *IEEE Trans. Syst., Man, Cybern.*, vol. 25 pp. 1194-1206, Aug. 1995.

[23] P. Gahinet, A. Nemirovski, A. Laub and M. Chilali, *The LMI Control Toolbox.* The MathWorks. Inc., 1995; also *in Proc. CDC*, 1994, pp. 2038-2041.